Environmental Science & Technology

Article

Cite This: Environ. Sci. Technol. 2019, 53, 13949−13958

pubs.acs.org/est

Connecting the Oxidative Potential of Secondary Organic Aerosols with Reactive Oxygen Species in Exposed Lung Cells

Pratiti Home Chowdhury,[†,§] Quanfu He,[†,§] Raanan Carmieli,[‡] Chunlin Li,[†] Yinon Rudich,[†] and Michal Pardo*[,†]

[†]Department of Earth and Planetary Sciences, and [‡]Department of Chemical Support Services, Weizmann Institute of Science, Rehovot 76100, Israel

Supporting Information

ABSTRACT: It has been hypothesized that the cytotoxicity of secondary organic aerosols (SOA) is mediated through the formation of reactive oxygen species (ROS) in the exposed cells. Here, lung epithelial cells (A549) residing at the air−liquid interface were exposed to proxies of anthropogenic and biogenic SOA that were photochemically aged under varying nitrogen oxide (NOx) concentrations in an oxidation flow reactor. The total organic peroxides and ROS radical content in the SOA were quantified by the iodometric spectrophotometric method and by continuous-wave electron paramagnetic resonance. The effect of the exposure was evaluated by measuring cell viability and cellular ROS production following the exposure. The results demonstrate that SOA that aged in the absence of NOx contained more ROS than fresh SOA and were more toxic toward the cells, while varying NOx conditions had no significant influence on levels of the ROS content in fresh SOA and their toxicity. Analysis of ROS in the exposed cells using flow cytometry showed a similar trend with the total ROS content in the SOA. This study provides a first and direct observation of such association.

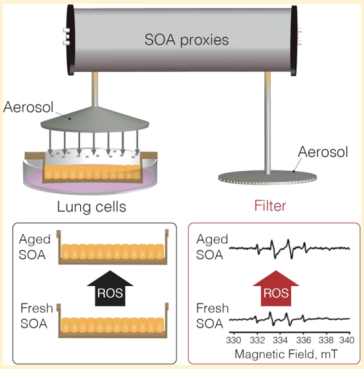

INTRODUCTION

Atmospheric aerosols (particulate matter, PM) originate from a wide variety of natural and anthropogenic emission sources, such as incomplete combustion of fossil fuels, biomass burning, volcanic eruptions, sea salt, the wind-driven or traffic-related suspension of road and mineral dust, and the oxidation of volatile organic compounds (VOC).[1−4] According to the World Health Organization and the Global Burden of Disease, atmospheric aerosols can induce adverse health effects upon inhalation and are considered among the top global health risks for mortality and morbidity.[1−6] Exposure to atmospheric particles has been associated with cardiorespiratory morbidity and mortality.[1,2,4,7] The health impacts and complex composition of atmospheric aerosols call for a deep understanding of the processes that are responsible for their toxicity.

Secondary organic aerosols (SOA) constitute a major fraction of atmospheric PM. They form in situ by the atmospheric oxidation of biogenic and anthropogenic VOCs. Biogenic VOCs emitted by the biosphere exceed the emission of VOCs from anthropogenic sources. During the day, VOCs are oxidized and photochemically aged, mostly by reactions with OH radicals and to a lesser extent by reactions with ozone[8−10] via the formation of highly oxygenated organic molecules (HOMs)[11] and other oxidized products. Organic peroxide radicals (RO_2) play a central role in atmospheric organic chemistry as well as in HOMs and SOA formation. The presence of nitrogen oxides (NOx = NO_2 + NO) can influence the formation mechanism and properties of SOA by competing with the HO_2 radical, OH radical, and RO_2 radicals, thus altering the bimolecular fate of the RO_2.[12−14] For example, in urban and polluted environments, high NOx concentrations lead to reactions of NO with RO_2, thus influencing the VOC oxidation pathways.[15,16] Chamber studies showed that NOx concentrations influence SOA production from a variety of compounds.[17] SOA characteristics such as hygroscopicity and optical properties may change significantly because of atmospheric photochemical aging under varying NOx conditions.[19−21] Despite recent progress in understanding the chemical and physical properties of SOA during aging under varying NOx conditions, the effect of SOA aging on the induction of adverse health effects is still unclear.[22]

The main toxicological mechanism induced by atmospheric PM exposure is thought to be by inducing oxidative stress that arises from an imbalance between oxidants and antioxidants.[7,23−27] It has been suggested that reactive oxygen species (ROS), which form by gas-phase and particle-phase oxidation reactions, can induce cell damage and induce basic cellular pathologies upon exposure.[25,28] Particle-bound ROS can be introduced through inhalation and may lead to an imbalance of ROS in the exposed cells or tissues.[7,28,29] For example, in acellular assays, the oxidative potential (OP) of naphthalene and α-pinene SOA showed high amounts of ROS (including OH, superoxide as well as carbon- and oxygen-

Received: July 24, 2019
Revised: October 23, 2019
Accepted: October 25, 2019
Published: October 25, 2019

DOI: 10.1021/acs.est.9b04449
Environ. Sci. Technol. 2019, 53, 13949−13958

centered organic radicals).[30] In addition, the OP of the ambient water-soluble fraction of $PM_{2.5}$ in the southeastern United States has been correlated with adverse health outcomes in this region.[29,31] A comprehensive recent study showed a connection between the ROS-generation potential of water-soluble $PM_{2.5}$ and epidemiological data, suggesting that oxidative stress is strongly associated with adverse health outcomes induced by exposure to $PM_{2.5}$. The authors of this study noted discrepancies in acellular OP measurement methods and emphasize the importance of identifying the chemical species responsible for determining the OP.[7] However, to date, a direct association between SOA-derived OP and OP in exposed cells has not been shown.

Different studies measured OP, peroxide, and radical contents in SOA using different methods and termed them accordingly. For example, ROS measured by on-line instruments were termed as aerosol-bound-ROS or particle-bound-ROS.[32,33] In addition, the aerosol-bound ROS measured by electron paramagnetic resonance (EPR) constitute a large part of the so-called environmentally persistent free radicals.[34] In the present study, we measured the total peroxide content in SOA and termed them as "SOA-bound-peroxides" following Mutzel et al., 2013. Similarly, we termed the radicals measured by EPR as "SOA-bound-radicals".

Only a few studies have investigated the toxic effects of SOA from different precursors, and specifically, the effect of SOA atmospheric aging on cytotoxicity.[8,35−38] In a previous study, we found that the aged naphthalene SOA is particularly cytotoxic toward lung epithelial cells.[36] We proposed that changes in the particles' OP have a direct link to the toxicological responses of the cells. However, no direct correlation was established to date between the type of SOA-bound radicals, their cytotoxicity, and the actual ROS content that form in the exposed cells. Therefore, to understand how photochemical processes of SOA affect their cytotoxicity mechanisms in lung cells, we employed an oxidation flow reactor (OFR) to photochemically age SOA under different NOx levels. Proxies of biogenic and anthropogenic precursors (α-pinene and naphthalene, respectively) were used in the generation of SOA and in the subsequent exposure of lung epithelial cells residing at the air−liquid interface (ALI).[39,40] In parallel, we investigated the SOA-bound ROS species via an iodometric spectroscopic method and with continuous-wave electron paramagnetic resonance (CW-EPR) using spin-trapping. ROS formation and oxidative status in the exposed cells were investigated using flow cytometry.

MATERIALS AND METHODS

Naphthalene and α-pinene SOA were produced in an oxidation flow reactor (OFR) in which high OH radical concentrations were achieved by the 254 nm photolysis of ozone followed by the reaction of $O(^1D)$ with water vapor. High OH exposure allows reaching higher oxidation levels than those usually encountered in photochemical simulation chamber studies. SOA were produced and photochemically aged by OH oxidation at zero and high levels of NOx. Previous studies have shown that SOA generated in this OFR chamber under well-defined conditions is a good surrogate for chamber-generated SOA with respect to the chemical composition, oxidation state, optical properties, and hygroscopicity.[36,41,42] In all cases, the SOA-bound peroxide and superoxide levels were measured by the iodometric−spectrophotometric method and CW-EPR. In parallel, lung epithelial cells residing at the ALI were exposed to the SOA using a CULTEX RFS system equipped with an electrostatic deposition device.[36,40]

SOA GENERATION AND CHARACTERIZATION

The experimental system is schematically shown in Supporting Information, Figure S1. SOA were generated by homogeneous nucleation, condensation, and aging following the OH oxidation of naphthalene (250 ppbv) and α-pinene (128 ppbv) in the presence/absence of NOx in a 13 L aluminum OFR.[42,43] The average residence time for gases and particles in the OFR was 180 s. The OH exposure was controlled by adjusting the OH radical concentration by optimizing the ultraviolet light intensity in the OFR at constant relative humidity (36 ± 2% at 22 °C). The details of the simulation of SOA formation and aging are given in Table S1. To simulate SOA produced in the presence of NOx, 2% N_2O by volume was added to the reactor. In the OFR, N_2O participates in a series of photochemical reactions to maintain relatively high mixing ratios of NO and NO_2, which serve as a homogeneous and attainable NOx source.[44] Measurements of SO_2 decay in the OFR allows to estimate the atmospheric equivalent aging time for "fresh" SOA from naphthalene and α-pinene to be 3.2 days under NOx-free and NOx conditions by assuming 1.5×10^6 molecules cm^{-3} as the daily average OH radical concentration. Utilizing a constrained model that considers the ozone concentrations, the residence time, and external reactivity of OH radicals,[45] the estimated atmospheric equivalent aging time of SOA produced under NOx-free conditions was ∼2 and ∼10 days for the "fresh" and the "aged" SOA, respectively (Table S1).

Gas-phase species, including ozone and NOx, were monitored during the exposure experiments. The size distributions of the generated SOA particles were measured by a scanning mobility particle sizer (SMPS, TSI). Non-refractory aerosol chemical composition and bulk elemental ratios (O/C and H/C ratios) were probed online with a high-resolution time-of-flight aerosol mass spectrometer (HR-ToF-AMS, Aerodyne Inc.). The dry particles' effective density was calculated from their aerodynamic diameter (measured by HR-ToF-AMS) and the mobility diameter (scanned by SMPS) to enable calculation of the exposed mass of the particles.

MEASUREMENTS OF TOTAL PEROXIDES IN SOA AND SOA-BOUND RADICALS

The total organic peroxides and ROS radicals in the SOA were quantified offline. Particles were collected on Teflon filters (0.45 μm pore size) for 0.5 h at a flow rate of 1 L min^{-1} and were used immediately after collection. The total organic peroxide content was measured photometrically using potassium iodide as described by Mutzel et al.[46] Briefly, half of a filter was used as a blank (measured without the addition of potassium iodide), and the second half was used for peroxide determination (with potassium iodide addition). All filters were extracted with 3 mL of ultrapure water by vortexing for 15 min at 2000 rpm. The extracted solution was filtered (Teflon syringe filter, 0.22 μm pore size) to remove undissolved components. The resulting filtrate was adjusted to pH 3.0 with acetic acid and purged with pure nitrogen gas for 5 min to remove dissolved oxygen (with capping). Potassium iodide (30 mg) was added to the peroxide test tube before gasification. After 1 h, the absorbance of the

DOI: 10.1021/acs.est.9b04449
Environ. Sci. Technol. 2019, 53, 13949−13958

pretreated solutions at λ = 351 nm was measured with a UV−vis spectrometer. The peroxide content was evaluated against a standard H_2O_2 calibration curve ranging from 6 to 100 μM.

DETERMINATION OF TOTAL ROS, OH, AND SUPEROXIDE RADICALS IN COLLECTED SOA

Filters were extracted with 1.5 mL of 40 mM 5-*tert*-butoxycarbonyl 5-methyl-1-pyrroline *N*-oxide (BMPO) in a vortex shaker for 10 min at 2000 rpm. The extract was filtered (Teflon syringe filter, 0.22 μm pore size) and immediately measured using a Bruker ELEXSYS E500 X-band EPR spectrometer equipped with a Bruker ER4102ST resonator in a Wilmad flat cell (WG-808-Q) for 100 scans at room temperature. The methodology was as previously published with minor modifications.[34,47] Briefly, EPR spectra were obtained with 512-point resolution at a microwave power of 20 mW, modulation amplitude of 0.1 mT, modulation frequency of 100 kHz, and sweep range of 20 mT.

The BMPO spin trap is most suitable for the detection of short-lived superoxide, hydroxyl, carbon-centered, and thiyl radicals by forming distinguishable adducts measurable by EPR spectroscopy.[34] The addition of superoxide dismutase (SOD), a superoxide scavenger, enables to distinguish between BMPO/OOH$^\bullet$ and BMPO/OH$^\bullet$ spin adducts. Based on the decrease in intensity, the amount of superoxide in the SOA was determined.

For quantitative analysis, the signal intensity was compared to a linear-fitted calibration curve obtained with known concentrations (1, 5, and 10 μM) of 3-carboxy-proxyl. The intensities of total BMPO-bound radicals, BMPO-OH radicals, and BMPO-OOH were quantified by double integration of the spectra, and the concentrations were then calculated using an established calibration curve. All EPR measurements were performed in triplicate. The quantified radical amounts were normalized by the SOA mass.

CELL CULTURE AND EXPOSURE SYSTEM

Human lung adenocarcinoma epithelial cell line A549 (ATCC catalog no. CCL-185) was grown in RPMI-1640 (Gibco, Thermofisher 65 Scientific, USA) supplemented with 2 mM glutamine, 10% fetal bovine serum (FBS), and 5 μg mL^{-1} penicillin−streptomycin (Biological Industries, Beit HaEmek Israel). A549 cells are widely used as an in vitro model for investigating the biological effects of PM.[48,49] The cells were exposed to SOA particles in an ALI exposure system (Cultex Inc.) for 4 h (the duration of the exposure was optimized between 1 and 6 h as described in the Supporting Information). For control, a similar setup of cells was exposed to particle-filtered flow. The exposure medium was supplemented with 100 mM *N*-(2-hydroxyethyl)piperazine-*N*′-ethanesulfonic acid (HEPES) without FBS. During the exposure, HEPES is added to the medium to maintain a physiological pH. FBS promotes cell growth, and it is omitted from the exposure medium to isolate the physiological responsiveness of the exposed cells. The post-incubation period was 18 h for the cell viability experiments and 4 h for the redox-state experiments. Further details of the cell exposure system are provided in the Supporting Information.

CELL VIABILITY MEASUREMENTS

Following the exposure, the viability of the exposed cells was measured using the WST-1 assay (Abcam). The WST-1 reagent measures cellular mitochondrial dehydrogenase activity by the cleavage of tetrazolium salt to formazan. This is a commonly used test in environmental research to determine the chemical cytotoxic potential.[50] The absorbance at 440 and 650 nm was measured in a microplate reader (VT 05404, Bio-Tech Instruments) after the cells was incubated with WST-1 for 30 min. The 650 nm absorbance was subtracted from the 440 nm absorbance to obtain the real absorbance. Then, the culture medium background was also subtracted to get the corrected absorbance. Finally, the cell viability percentage was calculated as follows:

$$\text{Cell viability (\%)} = 100(\text{Control-Sample})/\text{Control}$$

Cell viability is expressed compared to the incubator control which represents 100% cell viability.

Redox State of the Cells. The cellular redox state of the cells was evaluated by flow cytometry (LSR-II, BD Biosciences). Following 4 h of exposure to fresh/aged/NOx naphthalene and α-pinene SOA and 4 h of postexposure incubation, the cells were treated with 20 μM 2′,7′-dichlorodihydrofluorescein diacetate (H_2DCFDA) for 20 min at 37 °C in the dark. The total ROS was measured by H_2DCFDA (Thermo Fisher Scientific), which is more sensitive to H_2O_2 than to other free radicals. Ten thousand cells were measured with excitation/emission (Ex/Em) wavelengths of 495/529 nm. Superoxide anions (O_2^-) in the cells were also measured by flow cytometry using a ROS-Superoxide Detection Assay Kit (Abcam 139476). After 4 h of exposure to SOA and another 4 h of post-exposure incubation, the cells were incubated with the probe for the superoxide anion (provided by the kit). Ten thousand cells were measured at an Ex/Em of 550/620 nm. Unstained cells were used as the negative control, and cells exposed to 100 μM H_2O_2 were used as the positive control. H_2O_2 and superoxide inducer supplied by the manufacturer were used to determine the gating settings.

Statistical Analysis. All of the experiments were performed in triplicate and were repeated three times. Data are expressed as mean ± standard deviation (SD). The significance of the differences between each group was evaluated using Tukey's test in ANOVA, and differences were considered significant at $p < 0.05$ using Origin 2018.

RESULTS

SOA Generation and Characterization. In this study, the atmospheric equivalent aging days of naphthalene/α-pinene SOA were ∼3 days for fresh (produced with/without NOx, inferred from the SO_2 decay method) and ∼10 days (simulated by the model) for aged SOA. The particle masses for naphthalene/α-pinene SOA exposures were calculated using the measured particle density (1.1−1.4 g cm^{-3}, Table S2) and the SOA size distribution and are presented in Table S3. The SOA mass was at a level that moderately reduced cell viability.[36] Under all conditions, a relatively comparable SOA mass was achieved, except for α-pinene under NOx conditions, which had a lower SOA yield. This result is attributed to the competitive chemistry of RO_2 with NO compared to OH/HO_2/RO_2, which leads to a lower SOA mass yield for α-pinene.[17] Paur et al.[18] suggested that lifetime doses under realistic ambient conditions are equivalent to 6.6 μg cm^{-2} and can reach up to 29 μg cm^{-2}. Table S3 shows that the exposed particle mass is 8−11 μg cm^{-2}, corresponding to the upper limit of ambient conditions. With α-pinene-SOA under high

DOI: 10.1021/acs.est.9b04449
Environ. Sci. Technol. 2019, 53, 13949−13958

NOx conditions, the particle mass is lower (3.9 μg cm^{-2}) compared to the other conditions because of the limitation of our experimental setup.

The mass spectra of SOA produced under different conditions are shown in Figure S2. Fresh SOA mass spectra contain a large portion of $C_xH_y^+$ fragments, which indicates hydrocarbon-like organic aerosols. Predominant $C_xH_yO^+$ ions, the signature of carbonyl compounds, are fragments of typical early-generation oxidation products. Stronger signals for m/z 44 (CO_2^+, an indication of organic acids) and other more oxygenated $C_xH_yO_2^+$ ions were observed in the mass spectra of aged SOA. These results suggest that aged SOA produced at high OH exposure is dominated by higher generation oxidation products such as organic acids and organic peroxides. At the same time, the signal intensities of the prominent aromatic and carbonyl ions and cycloalkyls decreased. Notably, in naphthalene SOA, the set of signals at m/z 77, 91, 115, 119, 133, 147, and 160, which represent phenylalkyl fragments, drastically reduced during SOA production when NOx is added and upon aging. Peng et al. developed a model to simulate the atmospheric fate of RO_2 radicals in potential aerosol mass reactors.[13,51] Using their model, we estimated the relative contribution of the RO_2 + NO pathway to the RO_2 + HO_2 pathway in the fate of RO_2 radicals. In the presence of NOx, the ratios between these two pathways are 0.21 and 0.24 for naphthalene and α-pinene SOA, respectively. In the reactions of RO_2 + NO, large fractions of nitrogen-containing fragments were detected in the produced SOA. As suggested in previous studies, the NO^+/NO_2^+ ratio can be employed to estimate the portion of organic nitrates.[52,53] By using this method, the organic nitrate is estimated to be 87 and 78% of the total observed nitrate for the naphthalene- and α-pinene-derived SOA produced under NOx conditions. Assuming a molar mass of 250 g mol^{-1} for the organic nitrates and that each molecule contains one nitrate group, we estimated that the organic nitrate compromised ~40% of the mass for both types of SOA.

Total Organic Peroxides and the ROS Radical Content of SOA. Many factors such as the ROS content, photochemical aging, pH, and volatility can affect the OP of SOA.[7,9,54] Table S4 presents the total organic peroxide and ROS radical concentration in the SOA. In general, our results suggest that naphthalene SOA have a higher total peroxide content than α-pinene SOA, which is consistent with previous findings.[9,55] Aged naphthalene SOA contains higher total peroxides (13.80 nmol μg^{-1}) than fresh naphthalene SOA (5.17 nmol μg^{-1}), and α-pinene SOA show the same trend (7.39 vs 3.72 nmol μg^{-1}) (Table S4). These results indicate that atmospheric aging under NOx-free conditions leads to higher organic peroxide production in the SOA, which increases its OP and possibly also its cytotoxicity. These findings agree with previous studies showing that photochemical aging increases the OP of size-segregated airborne PM.[36,56] This observation is also consistent with the AMS results. Upon aging, the corresponding changes in the H/C to O/C ratios [Δ(H/C)/Δ(O/C)] were 0.03 and −0.70 for naphthalene- and α-pinene-derived SOA, respectively. These slopes are consistent with peroxide/alcohol formation and organic acid production.[57] For the SOA produced in the presence of NOx, the total peroxide levels are 5.56 and 3.87 nmol μg^{-1} for naphthalene and α-pinene SOA, respectively (Table S4). The peroxide content in these SOA types are similar to those produced in fresh SOA in the absence of NOx. These results are in agreement with Tuet et al. who showed that the OP of α-pinene, β-caryophyllene, and pentadecane SOA were similar regardless of reaction condition (with and without NOx).[38]

To explore the association between the peroxide content of SOA and ROS formation in exposed cells, the ROS content and OP of the SOA were investigated. The measured spectra of BMPO- and BMPO + SOD-treated SOA are shown in Figure S3. Only OH radicals and superoxide radicals were detected. The absolute molar content of total ROS radicals was higher in the α-pinene SOA than in the naphthalene SOA (Table S4), which is consistent with previous studies.[30,47] The relative content of these radicals in the SOA is shown in Figure 1. The

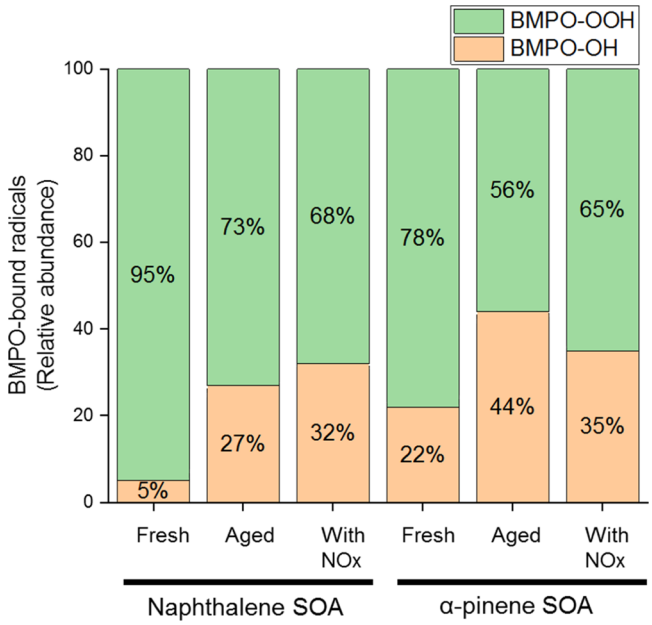

Figure 1. Relative contribution of BMPO-bound radicals in naphthalene and α-pinene SOA collected on Teflon filters. BMPO-OOH represents superoxide ions, and BMPO-OH represents OH radicals. The corresponding EPR signals are shown in Figure S3. The absolute values are given in Table S4.

observed formation of OH radicals (in the form of BMPO/OH) is most likely due to the decomposition of organic hydroperoxides (ROOH), which are formed via multigeneration gas-phase oxidation and autoxidation and account for the predominant fraction of SOA, especially for those produced from biogenic precursors.[14,46] Because of the low binding energy of the O−O bond, ROOH undergoes thermal homolytic cleavage, thus leading to the formation of OH radicals in SOA solutions.[47,58] The high production of OH radicals in the α-pinene SOA is attributed to the abundant amounts of organic hydroperoxide and high radical production yield.[59−61] In the naphthalene SOA, quinones such as the second-generation product 1,4-naphthoquinone (indicated by a molecular ion at m/z 158) and third-generation product 5-hydroxy-1,4-naphthoquinone (indicated by the molecular ion at m/z 174) were observed by HR-ToF-AMS. These quinones can undergo redox cycles that produce superoxide radicals.[62] This finding is consistent with our EPR results that superoxide was produced in the naphthalene SOA solution.

OH radicals produced by the SOA (measured with BMPO + SOD) account for 5, 27, and 32% of the peroxides in fresh,

DOI: 10.1021/acs.est.9b04449
Environ. Sci. Technol. 2019, 53, 13949−13958

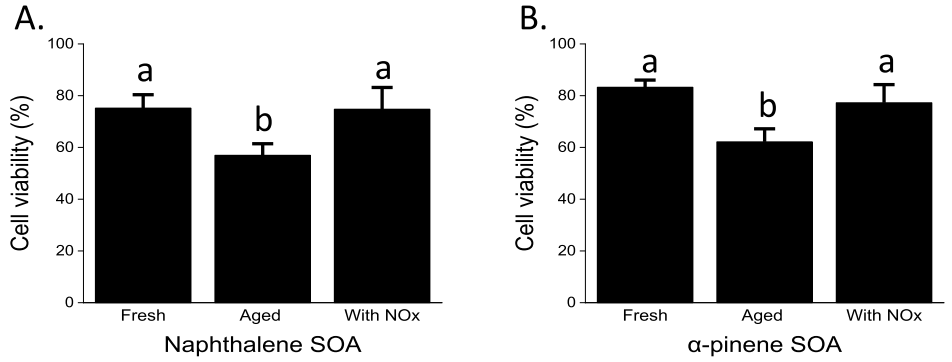

Figure 2. Cell viability measured by WST-1 assay following exposure to fresh, aged, and NOx addition naphthalene (A) and α-pinene (B) SOA. The data represent mean ± SD. Means with different letters are significantly different at $p < 0.05$ using the Tukey HSD test. All of these experiments were performed in triplicate and repeated twice.

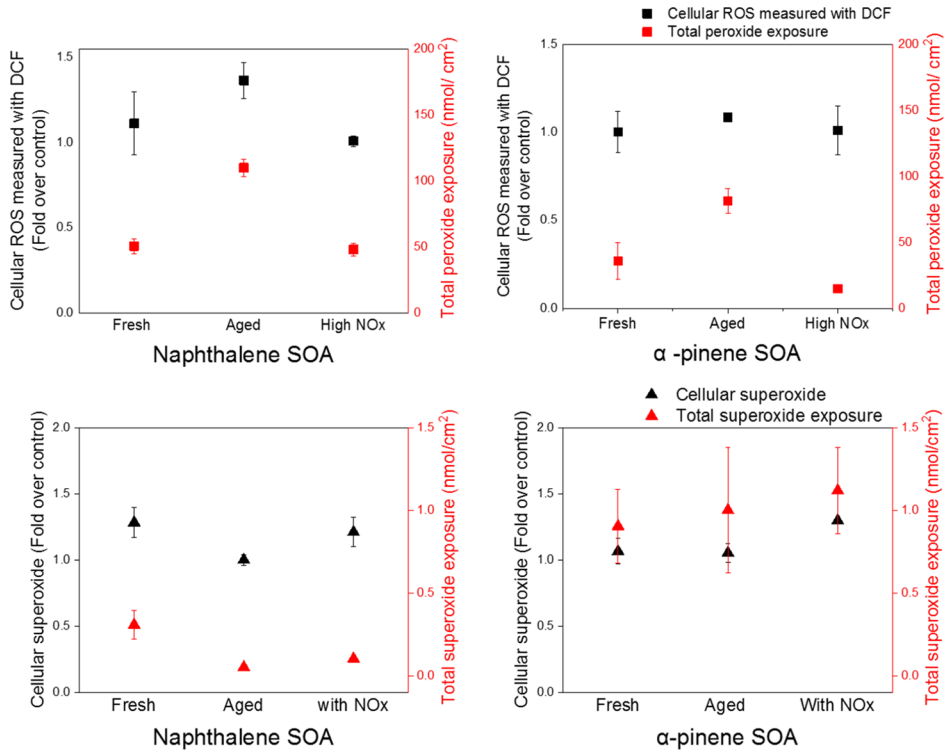

Figure 3. Association between particulate OP and cellular redox state (ROS and superoxide) after exposure to fresh, aged, and NOx addition (A,C) naphthalene and (B,D) α-pinene SOA. Total cellular ROS was measured by H_2DCFDA using flow cytometry (upper panel). Superoxide was measured by a superoxide kit using flow cytometry. Data are presented as the fold-change with respect to the control. The exposure was performed in triplicate and repeated at least two times. Data are expressed as the mean ± SD in terms of the fold change with respect to the negative control. The data represent mean ± SD.

aged, and with NOx naphthalene SOA, respectively, and for 22, 44, and 35% of the peroxides in fresh, aged, and with NOx α-pinene SOA, respectively. Under aged conditions, higher OH and HO_2 radical contents promote ROOH formation; thus, they can potentially increase OH radical production.[12,14] We noticed that the presence of NOx during SOA generation also leads to higher production of OH radicals by the SOA. Although NOx addition competes with OH and HO_2 radical reactions with RO_2 to suppress ROOH production, the products (nitrated compounds) from RO_2 + NO may be involved in further reactions that can affect radical production by the SOA solution. The superoxide percentage among the SOA-bound radicals is higher for naphthalene than α-pinene SOA; for naphthalene (fresh, aged, with NOx), the superoxide percentage is 95, 73, and 68%, respectively, and for α-pinene, the percentage is 78, 56, and 65%, respectively.

The source of the superoxide anion may vary between different SOA types. Tong et al. suggested that superoxide radicals can be generated by redox reactions of semiquinones.[47] This reaction may explain the observed high percentage of superoxide in the fresh naphthalene SOA. After aging, fragmentation occurs at higher OH radical concentrations, and more ring opening reactions occur, which decreased the quinone content but increased ROOH production. Thus, less superoxide and more OH radicals are generated by the aged naphthalene SOA. The superoxide anion radicals in α-pinene are formed by the thermal decomposition of ROOH, which is more labile.[54,63] However, the detailed

DOI: 10.1021/acs.est.9b04449
Environ. Sci. Technol. 2019, 53, 13949−13958

mechanism by which aging and NOx addition affect superoxide generation in α-pinene SOA is still unclear, and further studies are warranted.

Cell Viability and the Cellular Redox State after Exposure to SOA. PM exposure induces an array of health-related responses.[64−66] A growing line of evidence points to the involvement of SOA in inflammatory-related cascade, oxidative stress, and DNA damage.[36,67−69] In this study, the cell viability of lung epithelial cells toward SOA exposure was evaluated using WST-1 assay. The viability of lung epithelial cells decreased after exposure to all SOA conditions tested (fresh, aged, and with NOx) compared to the incubator control. Following exposure to fresh, aged, and NOx addition, naphthalene SOA cell viabilities were approximately 75, 57, and 75%, respectively (Figure 2). Following exposure to α-pinene SOA (fresh, aged, and with NOx), cell viability was 83, 62, and 77%, respectively (Figure 2). Aged SOA are more toxic than fresh SOA produced in the presence and absence of NOx for both naphthalene and α-pinene. This result is also supported by our previous study, where decreased cell viability for aged naphthalene and α-pinene SOA was observed.[36] No loss of cell viability was observed under particle-free flow.

It was previously shown that SOA production by OH photo-oxidation changes in the presence of NOx.[70] However, in general, the health-related effects have not been addressed. In this study, under the stated conditions, no significant changes in cell viability and cellular ROS due to NOx addition during SOA formation compared to SOA formed under NOx-free conditions were detected. This result is consistent with that of Tuet et al., who did not observe a significant effect on cellular ROS formation in murine alveolar macrophages when the SOA formation shifted between the RO_2 + HO_2/RO_2 + NO channels.[38] However, the exposure of BEAS-2B cells to isoprene SOA formed under high NOx conditions showed increased gene expression, which may be indicative of higher oxidative stress than under NOx-free conditions.[71] Thus far, the toxicity of SOA formed under NOx conditions is not clear, and further studies are recommended to draw a better understanding of their effects.

Using flow cytometry and 2′,7′-dichlorodihydrofluorescein diacetate (H_2DCFDA), we found that the exposed cells generated higher levels of ROS when exposed to aged naphthalene and α-pinene SOA than when exposed to the fresh SOA, similar to the trend observed for the SOA-bound ROS radicals and total peroxide levels (Figure 3). Table S3 summarizes the effective dose of SOA-bound peroxide and superoxide to which the cells were exposed. In agreement with Tuet et al.,[38] SOA produced in the presence of NOx did not induce higher cellular ROS compared to fresh SOA of a similar aging time that formed under NOx-free conditions (Figure 3). The total organic peroxides present in fresh and NOx condition of naphthalene SOA are similar. However, the total organic peroxide present in NOx condition of α-pinene SOA is 2.4 times lower than in fresh conditions. This is because of the low α-pinene SOA particle mass formed under NOx conditions. The total ROS levels measured in the cells after exposure to the SOA followed the trend of the total peroxide content in the SOA collected on the filters and the radical content analyzed by EPR. We found substantially higher levels of peroxides than that of radicals in the SOA extracts. This result suggests that the nonradical parts of SOA (possibly as H_2O_2 or other peroxides) are the most abundant ROS-producing species in the SOA (Table S4). This finding is consistent with the results of Tong et al., who reported that 62% of the total ROS was H_2O_2 when the SOA was extracted in water.[30] In addition, the DCF probe that was used to evaluate the total ROS within the cells has a higher affinity for H_2O_2.[72]

The superoxide levels measured in the collected SOA are similar under different SOA conditions except for α-pinene SOA formed under NOx conditions. Interestingly, the data show an association between the superoxide levels generated by the SOA and superoxide measured within the exposed cells (Figure 3C,D) and the decrease in cell viability (Figure 2).

DISCUSSION

In our previous work, we already showed that the higher production of peroxides due to photochemical aging is associated with higher expression of protective gene signaling.[36] We concluded that there is a trend of increasing ROS generation observed in cells exposed to SOA when SOA have higher peroxide concentrations. However, that study did not directly show the association. In addition, the previous study failed to identify which radicals or peroxide content of SOA are responsible for the higher ROS levels in the exposed cells. This gap led to the question, what types of radicals or peroxide increase in the cells (referred to as ROS in numerous publications). In this paper, we targeted the types of SOA-bound ROS that are responsible to the increase in the cellular ROS. Tong et al. 2018 previously addressed this question with acellular assay but not in a cellular system.[30] Our present study complements the Tong et al. paper by showing for the first time an association between the types of ROS and the cellular ROS production upon SOA exposure.

From the toxicological point of view, the direct and indirect formation of ROS and the induction of oxidative stress by inhaled particles are of special interest. A living cell requires a basal amount of ROS to perform its basic biological activities.[73,74] Under environmental stress, ROS levels can increase and consequently alter the cell's redox state and other cellular activities.[26,66] Cellular ROS include OH, H_2O_2, and superoxide ion (O_2^-), as well as nitro and organic radicals.[22] Several studies have shown that cells manifest different ROS-mediated oxidative stress responses upon the SOA or PM exposure.[24,38,75] It was recently shown that the amount of H_2O_2 and radicals, such as the superoxide anion, vary widely depending on the SOA precursor and its atmospheric aging processes.[30]

The observed association in this study between SOA peroxide levels and the total ROS detected in the cells (Figure 3A,B) suggests that peroxides generated by SOA promote H_2O_2 formation in the exposed cells. Because H_2O_2 can penetrate biological membranes,[76] it is directly related to cytotoxicity. The ROS levels measured in the cells and the higher peroxide content measured in the aged SOA exhibit a direct connection with cytotoxicity. This observation is consistent with our previous study which concluded that the cell viability of aged naphthalene SOA is related to its higher peroxide content.[36] This is also consistent with another study where exposure to PM increased the H_2O_2 released by nasal epithelial cells, thus contributing to oxidative stress.[77]

Superoxide is a highly reactive radical that can interact with other molecules/ions to generate secondary ROS (such as H_2O_2) directly or through enzyme/metal-catalyzed processes.[27] The cell death mechanism induced by exposure to $PM_{2.5}$ or its extracts in normal respiratory tissue or cells is often

DOI: 10.1021/acs.est.9b04449
Environ. Sci. Technol. 2019, 53, 13949−13958

mitochondria-mediated apoptosis.[78−80] Biologically, because the superoxide anion is often a byproduct of mitochondrial respiration, it is possible that the observed cell death following exposure to aged SOA and the corresponding low superoxide levels within the cells are mediated by mitochondrial dysfunction. Another possible explanation may be the high reactivity and short lifetime of the superoxide anion, which makes quantitative measurement difficult.[81]

This study provides a direct association between ROS found in SOA particles and the induction of ROS in exposed lung epithelial cells. In particular, we found that the concentration of peroxides in SOA increases with daytime atmospheric aging, with a corresponding decrease in cell viability and an increase in the total ROS content in the cells. The effect was stronger in naphthalene SOA than in α-pinene-derived SOA, possibly due to their higher peroxide levels. The effect of NOx addition on the ROS content in fresh SOA and in the exposed cells was also studied. We did not observe a clear NOx effect on the levels of ROS generated in fresh SOA and cells under the conditions studied here; hence, it is important to investigate how atmospheric aging under varying NOx levels affects the cytotoxicity of SOA. However, such conditions cannot be achieved in our experimental system. Although epidemiological and experimental studies have shown the detrimental effect of high NOx conditions,[65,82] it is necessary to design similar experiments to generate high NOx levels in highly aged conditions. Finally, Tong et al. showed that some ROS can react with lung lining fluid, thus diminishing the cells exposed to aerosol-bound ROS.[30] In our system, we could not simulate this effect, and we suggest that it should also be studied in a controlled way to better understand actual exposure to PM and its health effects.

■ ASSOCIATED CONTENT

Supporting Information

The Supporting Information is available free of charge on the ACS Publications website at DOI: 10.1021/acs.est.9b04449.

SOA generation in the OFR and OH exposure determination; cell culture, exposure system, and optimization of the exposure; summary of the initial conditions for SOA experiments; density and chemical composition (elemental ratios) of fresh, aged and with NOx conditions of naphthalene and α-pinene-derived SOA; exposed particle mass and ROS during the exposure experiment; SOA characterization: organic peroxide and ROS production; and schematic representation of the experiment (PDF)

■ AUTHOR INFORMATION

Corresponding Author

*E-mail: michal.levin@weizmann.ac.il (M.P.).

ORCID

Quanfu He: 0000-0002-3229-8206

Yinon Rudich: 0000-0003-3149-0201

Author Contributions

§P.H.C. and Q.H. made equal contributions.

Notes

The authors declare no competing financial interest.

■ ACKNOWLEDGMENTS

This study was partially funded by the German Israeli Science Foundation (#I-1338-307.8/2016) and is part of the Helmholtz International Lab aeroHEALTH (www.aerohealth.eu). The work was partially supported by a research grant from the Herbert L. Janowsky Lung Cancer Research Fund, Adam Glickman, Eric Gordon, Alex Rotzang, the David M. Polen Charitable Trust, The Benoziyo Endowment Fund for the Advancement of Science, and the Midwest Electron Microscope Project. Q.H. is supported by the Koshland Foundation and the Center for Planetary Sciences, Weizmann Institute of Science.

■ REFERENCES

(1) Shiraiwa, M.; Ueda, K.; Pozzer, A.; Lammel, G.; Kampf, C. J.; Fushimi, A.; Enami, S.; Arangio, A. M.; Fröhlich-Nowoisky, J.; Fujitani, Y.; Furuyama, A.; Lakey, P. S. J.; Lelieveld, J.; Lucas, K.; Morino, Y.; Pöschl, U.; Takahama, S.; Takami, A.; Tong, H.; Weber, B.; Yoshino, A.; Sato, K. Aerosol Health Effects from Molecular to Global Scales. *Environ. Sci. Technol.* **2017**, *51*, 13545−13567.

(2) Lim, S. S.; Vos, T.; Flaxman, A. D.; Danaei, G.; Shibuya, K.; Adair-Rohani, H.; AlMazroa, M. A.; Amann, M.; Anderson, H. R.; Andrews, K. G.; Aryee, M.; Atkinson, C.; Bacchus, L. J.; Bahalim, A. N.; Balakrishnan, K.; Balmes, J.; Barker-Collo, S.; Baxter, A.; Bell, M. L.; Blore, J. D.; Blyth, F.; Bonner, C.; Borges, G.; Bourne, R.; Boussinesq, M.; Brauer, M.; Brooks, P.; Bruce, N. G.; Brunekreef, B.; Bryan-Hancock, C.; Bucello, C.; Buchbinder, R.; Bull, F.; Burnett, R. T.; Byers, T. E.; Calabria, B.; Carapetis, J.; Carnahan, E.; Chafe, Z.; Charlson, F.; Chen, H.; Chen, J. S.; Cheng, A. T.-A.; Child, J. C.; Cohen, A.; Colson, K. E.; Cowie, B. C.; Darby, S.; Darling, S.; Davis, A.; Degenhardt, L.; Dentener, F.; Des Jarlais, D. C.; Devries, K.; Dherani, M.; Ding, E. L.; Dorsey, E. R.; Driscoll, T.; Edmond, K.; Ali, S. E.; Engell, R. E.; Erwin, P. J.; Fahimi, S.; Falder, G.; Farzadfar, F.; Ferrari, A.; Finucane, M. M.; Flaxman, S.; Fowkes, F. G. R.; Freedman, G.; Freeman, M. K.; Gakidou, E.; Ghosh, S.; Giovannucci, E.; Gmel, G.; Graham, K.; Grainger, R.; Grant, B.; Gunnell, D.; Gutierrez, H. R.; Hall, W.; Hoek, H. W.; Hogan, A.; Hosgood, H. D.; Hoy, D.; Hu, H.; Hubbell, B. J.; Hutchings, S. J.; Ibeanusi, S. E.; Jacklyn, G. L.; Jasrasaria, R.; Jonas, J. B.; Kan, H.; Kanis, J. A.; Kassebaum, N.; Kawakami, N.; Khang, Y.-H.; Khatibzadeh, S.; Khoo, J.-P.; Kok, C.; Laden, F.; Lalloo, R.; Lan, Q.; Lathlean, T.; Leasher, J. L.; Leigh, J.; Li, Y.; Lin, J. K.; Lipshultz, S. E.; London, S.; Lozano, R.; Lu, Y.; Mak, J.; Malekzadeh, R.; Mallinger, L.; Marcenes, W.; March, L.; Marks, R.; Martin, R.; McGale, P.; McGrath, J.; Mehta, S.; Memish, Z. A.; Mensah, G. A.; Merriman, T. R.; Micha, R.; Michaud, C.; Mishra, V.; Hanafiah, K. M.; Mokdad, A. A.; Morawska, L.; Mozaffarian, D.; Murphy, T.; Naghavi, M.; Neal, B.; Nelson, P. K.; Nolla, J. M.; Norman, R.; Olives, C.; Omer, S. B.; Orchard, J.; Osborne, R.; Ostro, B.; Page, A.; Pandey, K. D.; Parry, C. D. H.; Passmore, E.; Patra, J.; Pearce, N.; Pelizzari, P. M.; Petzold, M.; Phillips, M. R.; Pope, D.; Pope, C. A.; Powles, J.; Rao, M.; Razavi, H.; Rehfuess, E. A.; Rehm, J. T.; Ritz, B.; Rivara, F. P.; Roberts, T.; Robinson, C.; Rodriguez-Portales, J. A.; Romieu, I.; Room, R.; Rosenfeld, L. C.; Roy, A.; Rushton, L.; Salomon, J. A.; Sampson, U.; Sanchez-Riera, L.; Sanman, E.; Sapkota, A.; Seedat, S.; Shi, P.; Shield, K.; Shivakoti, R.; Singh, G. M.; Sleet, D. A.; Smith, E.; Smith, K. R.; Stapelberg, N. J. C.; Steenland, K.; Stöckl, H.; Stovner, L. J.; Straif, K.; Straney, L.; Thurston, G. D.; Tran, J. H.; Van Dingenen, R.; van Donkelaar, A.; Veerman, J. L.; Vijayakumar, L.; Weintraub, R.; Weissman, M. M.; White, R. A.; Whiteford, H.; Wiersma, S. T.; Wilkinson, J. D.; Williams, H. C.; Williams, W.; Wilson, N.; Woolf, A. D.; Yip, P.; Zielinski, J. M.; Lopez, A. D.; Murray, C. J. L.; Ezzati, M. A comparative risk assessment of burden of disease and injury attributable to 67 risk factors and risk factor clusters in 21 regions, 1990−2010: a systematic analysis for the Global Burden of Disease Study 2010. *Lancet* **2012**, *380*, 2224−2260.

(3) Lelieveld, J.; Barlas, C.; Giannadaki, D.; Pozzer, A. Model calculated global, regional and megacity premature mortality due to air pollution. *Atmos. Chem. Phys.* **2013**, *13*, 7023−7037.
(4) Lelieveld, J.; Klingmüller, K.; Pozzer, A.; Pöschl, U.; Fnais, M.; Daiber, A.; Münzel, T. Cardiovascular disease burden from ambient air pollution in Europe reassessed using novel hazard ratio functions. *Eur. Heart J.* **2019**, *40*, 1590−1596.
(5) Pöschl, U. Atmospheric aerosols: composition, transformation, climate and health effects. *Angew Chem. Int. Ed.* **2005**, *44*, 7520−7540.
(6) Cohen, A. J.; Brauer, M.; Burnett, R.; Anderson, H. R.; Frostad, J.; Estep, K.; Balakrishnan, K.; Brunekreef, B.; Dandona, L.; Dandona, R.; Feigin, V.; Freedman, G.; Hubbell, B.; Jobling, A.; Kan, H.; Knibbs, L.; Liu, Y.; Martin, R.; Morawska, L.; Pope, C. A., 3rd; Shin, H.; Straif, K.; Shaddick, G.; Thomas, M.; van Dingenen, R.; van Donkelaar, A.; Vos, T.; Murray, C. J. L.; Forouzanfar, M. H. Estimates and 25-year trends of the global burden of disease attributable to ambient air pollution: an analysis of data from the Global Burden of Diseases Study 2015. *Lancet* **2017**, *389*, 1907−1918.
(7) Bates, J. T.; Fang, T.; Verma, V.; Zeng, L.; Weber, R. J.; Tolbert, P. E.; Abrams, J. Y.; Sarnat, S. E.; Klein, M.; Mulholland, J. A.; Russell, A. G. Review of Acellular Assays of Ambient Particulate Matter Oxidative Potential: Methods and Relationships with Composition, Sources, and Health Effects. *Environ. Sci. Technol.* **2019**, *53*, 4003−4019.
(8) Wang, Y.; Kim, H.; Paulson, S. E. Hydrogen peroxide generation from α- and β-pinene and toluene secondary organic aerosols. *Atmos. Environ.* **2011**, *45*, 3149−3156.
(9) Mertes, P.; Pfaffenberger, L.; Dommen, J.; Kalberer, M.; Baltensperger, U. Development of a sensitive long path absorption photometer to quantify peroxides in aerosol particles (Peroxide-LOPAP). *Atmos. Meas. Tech.* **2012**, *5*, 2339−2348.
(10) Zhang, X.; McVay, R. C.; Huang, D. D.; Dalleska, N. F.; Aumont, B.; Flagan, R. C.; Seinfeld, J. H. Formation and evolution of molecular products in alpha-pinene secondary organic aerosol. *Proc. Natl. Acad. Sci. U.S.A.* **2015**, *112*, 14168−14173.
(11) Bianchi, F.; Kurtén, T.; Riva, M.; Mohr, C.; Rissanen, M. P.; Roldin, P.; Berndt, T.; Crounse, J. D.; Wennberg, P. O.; Mentel, T. F.; Wildt, J.; Junninen, H.; Jokinen, T.; Kulmala, M.; Worsnop, D. R.; Thornton, J. A.; Donahue, N.; Kjaergaard, H. G.; Ehn, M. Highly Oxygenated Organic Molecules (HOM) from Gas-Phase Autoxidation Involving Peroxy Radicals: A Key Contributor to Atmospheric Aerosol. *Chem. Rev.* **2019**, *119*, 3472−3509.
(12) Orlando, J. J.; Tyndall, G. S. Laboratory studies of organic peroxy radical chemistry: an overview with emphasis on recent issues of atmospheric significance. *Chem. Soc. Rev.* **2012**, *41*, 6294−6317.
(13) Peng, Z.; Lee-Taylor, J.; Orlando, J. J.; Tyndall, G. S.; Jimenez, J. L. Organic peroxy radical chemistry in oxidation flow reactors and environmental chambers and their atmospheric relevance. *Atmos. Chem. Phys.* **2019**, *19*, 813−834.
(14) Ziemann, P. J.; Atkinson, R. Kinetics, products, and mechanisms of secondary organic aerosol formation. *Chem. Soc. Rev.* **2012**, *41*, 6582−6605.
(15) Barket, D. J.; Grossenbacher, J. W.; Hurst, J. M.; Shepson, P. B.; Olszyna, K.; Thornberry, T.; Carroll, M. A.; Roberts, J.; Stroud, C.; Bottenheim, J.; Biesenthal, T., A study of the NOx dependence of isoprene oxidation. *J. Geophys. Res.: Atmos.* **2004**, *109*, (), doi: DOI: 10.1029/2003JD003965.
(16) Madronich, S. Chemical evolution of gaseous air pollutants down-wind of tropical megacities: Mexico City case study. *Atmos. Environ.* **2006**, *40*, 6012−6018.
(17) Ng, N. L.; Chhabra, P. S.; Chan, A. W. H.; Surratt, J. D.; Kroll, J. H.; Kwan, A. J.; McCabe, D. C.; Wennberg, P. O.; Sorooshian, A.; Murphy, S. M.; Dalleska, N. F.; Flagan, R. C.; Seinfeld, J. H. Effect of NOx level on secondary organic aerosol (SOA) formation from the photooxidation of terpenes. *Atmos. Chem. Phys.* **2007**, *7*, 5159−5174.
(18) Paur, H.-R.; Cassee, F. R.; Teeguarden, J.; Fissan, H.; Diabate, S.; Aufderheide, M.; Kreyling, W. G.; Hänninen, O.; Kasper, G.; Riediker, M.; Rothen-Rutishauser, B.; Schmid, O. In-vitro cell exposure studies for the assessment of nanoparticle toxicity in the lung, A dialog between aerosol science and biology. *J. Aerosol Sci.* **2011**, *42*, 668−692.
(19) Sarrafzadeh, M.; Wildt, J.; Pullinen, I.; Springer, M.; Kleist, E.; Tillmann, R.; Schmitt, S. H.; Wu, C.; Mentel, T. F.; Zhao, D.; Hastie, D. R.; Kiendler-Scharr, A. Impact of NOx and OH on secondary organic aerosol formation from β-pinene photooxidation. *Atmos. Chem. Phys.* **2016**, *16*, 11237−11248.
(20) Denjean, C.; Formenti, P.; Picquet-Varrault, B.; Pangui, E.; Zapf, P.; Katrib, Y.; Giorio, C.; Tapparo, A.; Monod, A.; Temime-Roussel, B.; Decorse, P.; Mangeney, C.; Doussin, J. F. Relating hygroscopicity and optical properties to chemical composition and structure of secondary organic aerosol particles generated from the ozonolysis of α-pinene. *Atmos. Chem. Phys.* **2015**, *15*, 3339−3358.
(21) He, Q.; Bluvshtein, N.; Segev, L.; Meidan, D.; Flores, J. M.; Brown, S. S.; Brune, W.; Rudich, Y. Evolution of the Complex Refractive Index of Secondary Organic Aerosols during Atmospheric Aging. *Environ. Sci. Technol.* **2018**, *52*, 3456−3465.
(22) Pöschl, U.; Shiraiwa, M. Multiphase Chemistry at the Atmosphere-Biosphere Interface Influencing Climate and Public Health in the Anthropocene. *Chem. Rev.* **2015**, *115*, 4440−4475.
(23) Bates, J. T.; Weber, R. J.; Abrams, J.; Verma, V.; Fang, T.; Klein, M.; Strickland, M. J.; Sarnat, S. E.; Chang, H. H.; Mulholland, J. A.; Tolbert, P. E.; Russell, A. G. Reactive Oxygen Species Generation Linked to Sources of Atmospheric Particulate Matter and Cardiorespiratory Effects. *Environ. Sci. Technol.* **2015**, *49*, 13605−13612.
(24) Landreman, A. P.; Shafer, M. M.; Hemming, J. C.; Hannigan, M. P.; Schauer, J. J. A Macrophage-Based Method for the Assessment of the Reactive Oxygen Species (ROS) Activity of Atmospheric Particulate Matter (PM) and Application to Routine (Daily-24 h) Aerosol Monitoring Studies. *Aerosol Sci. Technol.* **2008**, *42*, 946−957.
(25) Lodovici, M.; Bigagli, E. Oxidative stress and air pollution exposure. *J. Toxicol.* **2011**, *2011*, 487074.
(26) Mittler, R. ROS Are Good. *Trends Plant Sci.* **2017**, *22*, 11−19.
(27) Valko, M.; Rhodes, C. J.; Moncol, J.; Izakovic, M.; Mazur, M. Free radicals, metals and antioxidants in oxidative stress-induced cancer. *Chem. Biol. Interact.* **2006**, *160*, 1−40.
(28) Wang, S.; Ye, J.; Soong, R.; Wu, B.; Yu, L.; Simpson, A. J.; Chan, A. W. H. Relationship between chemical composition and oxidative potential of secondary organic aerosol from polycyclic aromatic hydrocarbons. *Atmos. Chem. Phys.* **2018**, *18*, 3987−4003.
(29) Fang, T.; Verma, V.; Bates, J. T.; Abrams, J.; Klein, M.; Strickland, M. J.; Sarnat, S. E.; Chang, H. H.; Mulholland, J. A.; Tolbert, P. E.; Russell, A. G.; Weber, R. J. Oxidative potential of ambient water-soluble PM2.5 in the southeastern United States: contrasts in sources and health associations between ascorbic acid (AA) and dithiothreitol (DTT) assays. *Atmos. Chem. Phys.* **2016**, *16*, 3865−3879.
(30) Tong, H.; Lakey, P. S. J.; Arangio, A. M.; Socorro, J.; Shen, F.; Lucas, K.; Brune, W. H.; Poschl, U.; Shiraiwa, M. Reactive Oxygen Species Formed by Secondary Organic Aerosols in Water and Surrogate Lung Fluid. *Environ. Sci. Technol.* **2018**, *52*, 11642−11651.
(31) Bates, J. T.; Weber, R. J.; Verma, V.; Fang, T.; Ivey, C.; Liu, C.; Sarnat, S. E.; Chang, H. H.; Mulholland, J. A.; Russell, A. Source impact modeling of spatiotemporal trends in PM2.5 oxidative potential across the eastern United States. *Atmos. Environ.* **2018**, *193*, 158−167.
(32) Wragg, F. P. H.; Fuller, S. J.; Freshwater, R.; Green, D. C.; Kelly, F. J.; Kalberer, M. An automated online instrument to quantify aerosol-bound reactive oxygen species (ROS) for ambient measurement and health-relevant aerosol studies. *Atmos. Meas. Tech.* **2016**, *9*, 4891−4900.
(33) Fuller, S. J.; Wragg, F. P. H.; Nutter, J.; Kalberer, M. Comparison of on-line and off-line methods to quantify reactive oxygen species (ROS) in atmospheric aerosols. *Atmospheric Environment* **2014**, *92*, 97−103.
(34) Arangio, A. M.; Tong, H.; Socorro, J.; Pöschl, U.; Shiraiwa, M. Quantification of environmentally persistent free radicals and reactive

DOI: 10.1021/acs.est.9b04449
Environ. Sci. Technol. 2019, 53, 13949−13958

oxygen species in atmospheric aerosol particles. *Atmos. Chem. Phys.* **2016**, *16*, 13105−13119.
(35) Mauderly, J. L.; Chow, J. C. Health effects of organic aerosols. *Inhal. Toxicol.* **2008**, *20*, 257−288.
(36) Chowdhury, P. H.; He, Q.; Lasitza Male, T.; Brune, W. H.; Rudich, Y.; Pardo, M. Exposure of Lung Epithelial Cells to Photochemically Aged Secondary Organic Aerosol Shows Increased Toxic Effects. *Environ. Sci. Technol. Lett.* **2018**, *5*, 424−430.
(37) Lin, Y.-H.; Arashiro, M.; Clapp, P. W.; Cui, T.; Sexton, K. G.; Vizuete, W.; Gold, A.; Jaspers, I.; Fry, R. C.; Surratt, J. D. Gene Expression Profiling in Human Lung Cells Exposed to Isoprene-Derived Secondary Organic Aerosol. *Environ. Sci. Technol.* **2017**, *51*, 8166−8175.
(38) Tuet, W. Y.; Chen, Y.; Fok, S.; Champion, J. A.; Ng, N. L. Inflammatory responses to secondary organic aerosols (SOA) generated from biogenic and anthropogenic precursors. *Atmos. Chem. Phys.* **2017**, *17*, 11423−11440.
(39) Aufderheide, M.; Förster, C.; Beshay, M.; Branscheid, D.; Emura, M. A new computer-controlled air-liquid interface cultivation system for the generation of differentiated cell cultures of the airway epithelium. *Exp. Toxicol. Pathol.* **2016**, *68*, 77−87.
(40) Aufderheide, M.; Halter, B.; Mohle, N.; Hochrainer, D. The CULTEX RFS: a comprehensive technical approach for the in vitro exposure of airway epithelial cells to the particulate matter at the air-liquid interface. *BioMed Res. Int.* **2013**, *2013*, 734137.
(41) Bruns, E. A.; El Haddad, I.; Keller, A.; Klein, F.; Kumar, N. K.; Pieber, S. M.; Corbin, J. C.; Slowik, J. G.; Brune, W. H.; Baltensperger, U.; Prévôt, A. S. H. Inter-comparison of laboratory smog chamber and flow reactor systems on organic aerosol yield and composition. *Atmos. Meas. Tech.* **2015**, *8*, 2315−2332.
(42) Lambe, A. T.; Ahern, A. T.; Williams, L. R.; Slowik, J. G.; Wong, J. P. S.; Abbatt, J. P. D.; Brune, W. H.; Ng, N. L.; Wright, J. P.; Croasdale, D. R.; Worsnop, D. R.; Davidovits, P.; Onasch, T. B. Characterization of aerosol photooxidation flow reactors: heterogeneous oxidation, secondary organic aerosol formation and cloud condensation nuclei activity measurements. *Atmos. Meas. Tech.* **2011**, *4*, 445−461.
(43) Kang, E.; Root, M. J.; Toohey, D. W.; Brune, W. H. Introducing the concept of Potential Aerosol Mass (PAM). *Atmos. Chem. Phys.* **2007**, *7*, 5727−5744.
(44) Lambe, A.; Massoli, P.; Zhang, X.; Canagaratna, M.; Nowak, J.; Daube, C.; Yan, C.; Nie, W.; Onasch, T.; Jayne, J.; Kolb, C.; Davidovits, P.; Worsnop, D.; Brune, W. Controlled nitric oxide production via O1D +N2O reactions for use in oxidation flow reactor studies. *Atmos. Meas. Tech.* **2017**, *10*, 2283−2298.
(45) Peng, Z.; Day, D. A.; Ortega, A. M.; Palm, B. B.; Hu, W.; Stark, H.; Li, R.; Tsigaridis, K.; Brune, W. H.; Jimenez, J. L. Non-OH chemistry in oxidation flow reactors for the study of atmospheric chemistry systematically examined by modeling. *Atmos. Chem. Phys.* **2016**, *16*, 4283−4305.
(46) Mutzel, A.; Rodigast, M.; Iinuma, Y.; Böge, O.; Herrmann, H. An improved method for the quantification of SOA bound peroxides. *Atmos. Environ.* **2013**, *67*, 365−369.
(47) Tong, H.; Lakey, P. S. J.; Arangio, A. M.; Socorro, J.; Kampf, C. J.; Berkemeier, T.; Brune, W. H.; Pöschl, U.; Shiraiwa, M. Reactive oxygen species formed in aqueous mixtures of secondary organic aerosols and mineral dust influencing cloud chemistry and public health in the Anthropocene. *Faraday Discuss.* **2017**, *200*, 251−270.
(48) Kim, W.; Jeong, S.-C.; Shin, C.-y.; Song, M.-K.; Cho, Y.; Lim, J.-h.; Gye, M. C.; Ryu, J.-C. A study of cytotoxicity and genotoxicity of particulate matter (PM2.5) in human lung epithelial cells (A549). *Mol. Cell. Toxicol.* **2018**, *14*, 163−172.
(49) Bitterle, E.; Karg, E.; Schroeppel, A.; Kreyling, W. G.; Tippe, A.; Ferron, G. A.; Schmid, O.; Heyder, J.; Maier, K. L.; Hofer, T. Dose-controlled exposure of A549 epithelial cells at the air-liquid interface to airborne ultrafine carbonaceous particles. *Chemosphere* **2006**, *65*, 1784−1790.
(50) Landkocz, Y.; Ledoux, F.; André, V.; Cazier, F.; Genevray, P.; Dewaele, D.; Martin, P. J.; Lepers, C.; Verdin, A.; Courcot, L.; Boushina, S.; Sichel, F.; Gualtieri, M.; Shirali, P.; Courcot, D.; Billet, S. Fine and ultrafine atmospheric particulate matter at a multi-influenced urban site: Physicochemical characterization, mutagenicity and cytotoxicity. *Environ. Pollut.* **2017**, *221*, 130−140.
(51) Peng, Z.; Palm, B. B.; Day, D. A.; Talukdar, R. K.; Hu, W.; Lambe, A. T.; Brune, W. H.; Jimenez, J. L. Model Evaluation of New Techniques for Maintaining High-NO Conditions in Oxidation Flow Reactors for the Study of OH-Initiated Atmospheric Chemistry. *ACS Earth Space Chem.* **2018**, *2*, 72−86.
(52) Kiendler-Scharr, A.; Mensah, A. A.; Friese, E.; Topping, D.; Nemitz, E.; Prevot, A. S. H.; Äijälä, M.; Allan, J.; Canonaco, F.; Canagaratna, M.; Carbone, S.; Crippa, M.; Dall Osto, M.; Day, D. A.; De Carlo, P.; Di Marco, C. F.; Elbern, H.; Eriksson, A.; Freney, E.; Hao, L.; Herrmann, H.; Hildebrandt, L.; Hillamo, R.; Jimenez, J. L.; Laaksonen, A.; McFiggans, G.; Mohr, C.; O'Dowd, C.; Otjes, R.; Ovadnevaite, J.; Pandis, S. N.; Poulain, L.; Schlag, P.; Sellegri, K.; Swietlicki, E.; Tiitta, P.; Vermeulen, A.; Wahner, A.; Worsnop, D.; Wu, H.-C. Ubiquity of organic nitrates from nighttime chemistry in the European submicron aerosol. *Geophys. Res. Lett.* **2016**, *43*, 7735−7744.
(53) Farmer, D. K.; Matsunaga, A.; Docherty, K. S.; Surratt, J. D.; Seinfeld, J. H.; Ziemann, P. J.; Jimenez, J. L. Response of an aerosol mass spectrometer to organonitrates and organosulfates and implications for atmospheric chemistry. *Proc. Natl. Acad. Sci. U.S.A.* **2010**, *107*, 6670−6675.
(54) Kautzman, K. E.; Surratt, J. D.; Chan, M. N.; Chan, A. W. H.; Hersey, S. P.; Chhabra, P. S.; Dalleska, N. F.; Wennberg, P. O.; Flagan, R. C.; Seinfeld, J. H. Chemical composition of gas- and aerosol-phase products from the photooxidation of naphthalene. *J. Phys. Chem. A* **2010**, *114*, 913−934.
(55) Tuet, W. Y.; Chen, Y.; Xu, L.; Fok, S.; Gao, D.; Weber, R. J.; Ng, N. L. Chemical oxidative potential of secondary organic aerosol (SOA) generated from the photooxidation of biogenic and anthropogenic volatile organic compounds. *Atmos. Chem. Phys.* **2017**, *17*, 839−853.
(56) Saffari, A.; Daher, N.; Ruprecht, A.; De Marco, C.; Pozzi, P.; Boffi, R.; Hamad, S. H.; Shafer, M. M.; Schauer, J. J.; Westerdahl, D.; Sioutas, C. Particulate metals and organic compounds from electronic and tobacco-containing cigarettes: comparison of emission rates and secondhand exposure. *Environ. Sci.: Processes Impacts* **2014**, *16*, 2259−2267.
(57) Heald, C. L.; Kroll, J. H.; Jimenez, J. L.; Docherty, K. S.; DeCarlo, P. F.; Aiken, A. C.; Chen, Q.; Martin, S. T.; Farmer, D. K.; Artaxo, P. A simplified description of the evolution of organic aerosol composition in the atmosphere. *Geophys. Res. Lett.* **2010**, *37*, L08803.
(58) Tong, H.; Arangio, A. M.; Lakey, P. S. J.; Berkemeier, T.; Liu, F.; Kampf, C. J.; Brune, W. H.; Pöschl, U.; Shiraiwa, M. Hydroxyl radicals from secondary organic aerosol decomposition in water. *Atmos. Chem. Phys.* **2016**, *16*, 1761−1771.
(59) Docherty, K. S.; Wu, W.; Lim, Y. B.; Ziemann, P. J. Contributions of organic peroxides to secondary aerosol formed from reactions of monoterpenes with O-3. *Environ. Sci. Technol.* **2005**, *39*, 4049−4059.
(60) Badali, K. M.; Zhou, S.; Aljawhary, D.; Antiñolo, M.; Chen, W. J.; Lok, A.; Mungall, E.; Wong, J. P. S.; Zhao, R.; Abbatt, J. P. D. Formation of hydroxyl radicals from photolysis of secondary organic aerosol material. *Atmos. Chem. Phys.* **2015**, *15*, 7831−7840.
(61) Tong, H.; Zhang, Y.; Filippi, A.; Wang, T.; Li, C.; Liu, F.; Leppla, D.; Kourtchev, I.; Wang, K.; Keskinen, H.-M.; Levula, J. T.; Arangio, A. M.; Shen, F.; Ditas, F.; Martin, S. T.; Artaxo, P.; Godoi, R. H. M.; Yamamoto, C. I.; de Souza, R. A. F.; Huang, R.-J.; Berkemeier, T.; Wang, Y.; Su, H.; Cheng, Y.; Pope, F. D.; Fu, P.; Yao, M.; Pöhlker, C.; Petäjä, T.; Kulmala, M.; Andreae, M. O.; Shiraiwa, M.; Pöschl, U.; Hoffmann, T.; Kalberer, M., Radical Formation by Fine Particulate Matter Associated with Highly Oxygenated Molecules. *Environ. Sci. Technol.* **2019** DOI: 10.1021/acs.est.9b05149.
(62) McWhinney, R. D.; Zhou, S.; Abbatt, J. P. D. Naphthalene SOA: redox activity and naphthoquinone gas-particle partitioning. *Atmos. Chem. Phys.* **2013**, *13*, 9731−9744.

DOI: 10.1021/acs.est.9b04449
Environ. Sci. Technol. 2019, 53, 13949−13958

(63) Eddingsaas, N. C.; Loza, C. L.; Yee, L. D.; Chan, M.; Schilling, K. A.; Chhabra, P. S.; Seinfeld, J. H.; Wennberg, P. O. α-pinene photooxidation under controlled chemical conditions - Part 2: SOA yield and composition in low- and high-NOx environments. *Atmos. Chem. Phys.* **2012**, *12*, 7413−7427.
(64) Brook, R. D.; Rajagopalan, S.; Pope, C. A., 3rd; Brook, J. R.; Bhatnagar, A.; Diez-Roux, A. V.; Holguin, F.; Hong, Y.; Luepker, R. V.; Mittleman, M. A.; Peters, A.; Siscovick, D.; Smith, S. C., Jr.; Whitsel, L.; Kaufman, J. D.; American Heart Association Council on, E.; Prevention, C. o. t. K. i. C. D.; Council on Nutrition, P. A. Metabolism, Particulate matter air pollution and cardiovascular disease: An update to the scientific statement from the American Heart Association. *Circulation* **2010**, *121*, 2331−2378.
(65) Guarnieri, M.; Balmes, J. R. Outdoor air pollution and asthma. *Lancet* **2014**, *383*, 1581−1592.
(66) Chowdhury, P. H.; Okano, H.; Honda, A.; Kudou, H.; Kitamura, G.; Ito, S.; Ueda, K.; Takano, H. Aqueous and organic extract of PM2.5 collected in different seasons and cities of Japan differently affect respiratory and immune systems. *Environ. Pollut.* **2018**, *235*, 223−234.
(67) Peixoto, M. S.; de Oliveira Galvão, M. F.; Batistuzzo de Medeiros, S. R. Cell death pathways of particulate matter toxicity. *Chemosphere* **2017**, *188*, 32−48.
(68) Tuet, W. Y.; Chen, Y.; Fok, S.; Gao, D.; Weber, R. J.; Champion, J. A.; Ng, N. L. Chemical and cellular oxidant production induced by naphthalene secondary organic aerosol (SOA): effect of redox-active metals and photochemical aging. *Sci. Rep.* **2017**, *7*, 15157.
(69) Kawanishi, S.; Ohnishi, S.; Ma, N.; Hiraku, Y.; Murata, M. Crosstalk between DNA Damage and Inflammation in the Multiple Steps of Carcinogenesis. *Int. J. Mol. Sci.* **2017**, *18*, 1808.
(70) Xu, J.; Griffin, R. J.; Liu, Y.; Nakao, S.; Cocker, D. R. Simulated impact of NOx on SOA formation from oxidation of toluene and m-xylene. *Atmos. Environ.* **2015**, *101*, 217−225.
(71) Lin, Y.-H.; Arashiro, M.; Martin, E.; Chen, Y.; Zhang, Z.; Sexton, K. G.; Gold, A.; Jaspers, I.; Fry, R. C.; Surratt, J. D. Isoprene-Derived Secondary Organic Aerosol Induces the Expression of Oxidative Stress Response Genes in Human Lung Cells. *Environ. Sci. Technol. Lett.* **2016**, *3*, 250−254.
(72) Carter, W. O.; Narayanan, P. K.; Robinson, J. P. Intracellular hydrogen peroxide and superoxide anion detection in endothelial cells. *J. Leukoc. Biol.* **1994**, *55*, 253−258.
(73) Abbas, I.; Garçon, G.; Saint-Georges, F.; Billet, S.; Verdin, A.; Gosset, P.; Mulliez, P.; Shirali, P. Occurrence of molecular abnormalities of cell cycle in L132 cells after in vitro short-term exposure to air pollution PM(2.5). *Chem. Biol. Interact.* **2010**, *188*, 558−565.
(74) Forman, H. J.; Maiorino, M.; Ursini, F. Signaling functions of reactive oxygen species. *Biochemistry* **2010**, *49*, 835−842.
(75) Tuet, W. Y.; Fok, S.; Verma, V.; Tagle Rodriguez, M. S.; Grosberg, A.; Champion, J. A.; Ng, N. L. Dose-dependent intracellular reactive oxygen and nitrogen species (ROS/RNS) production from particulate matter exposure: comparison to oxidative potential and chemical composition. *Atmos. Environ.* **2016**, *144*, 335−344.
(76) Silva, J. P.; Coutinho, O. P. Free radicals in the regulation of damage and cell death − basic mechanisms and prevention. *Drug Discov. Ther.* **2010**, *4*, 144−167.
(77) Cho, D.-Y.; Le, W.; Bravo, D. T.; Hwang, P. H.; Illek, B.; Fischer, H.; Nayak, J. V. Air pollutants cause release of hydrogen peroxide and interleukin-8 in a human primary nasal tissue culture model. *Int. Forum Allergy Rhinol.* **2014**, *4*, 966−971.
(78) Lavrich, K. S.; Corteselli, E. M.; Wages, P. A.; Bromberg, P. A.; Simmons, S. O.; Gibbs-Flournoy, E. A.; Samet, J. M. Investigating mitochondrial dysfunction in human lung cells exposed to redox-active PM components. *Toxicol. Appl. Pharmacol.* **2018**, *342*, 99−107.
(79) Jin, S.; Diano, S. Mitochondrial Dynamics and Hypothalamic Regulation of Metabolism. *Endocrinology* **2018**, *159*, 3596−3604.
(80) Pardo, M.; Xu, F.; Shemesh, M.; Qiu, X.; Barak, Y.; Zhu, T.; Rudich, Y. Nrf2 protects against diverse PM2.5 components-induced mitochondrial oxidative damage in lung cells. *Sci. Total Environ.* **2019**, *669*, 303−313.
(81) Hayyan, M.; Hashim, M. A.; AlNashef, I. M. Superoxide Ion: Generation and Chemical Implications. *Chem. Rev.* **2016**, *116*, 3029−3085.
(82) César, A. C. G.; Carvalho, J. A., Jr.; Nascimento, L. F. C. Association between NOx exposure and deaths caused by respiratory diseases in a medium-sized Brazilian city. *Braz. J. Med. Biol. Res.* **2015**, *48*, 1130−1135.

DOI: 10.1021/acs.est.9b04449
Environ. Sci. Technol. 2019, 53, 13949−13958

Supporting information

Connecting the oxidative potential of secondary organic aerosols to their cytotoxicity

Pratiti Home Chowdhury[†,§], Quanfu He[†,§], Raanan Carmieli[‡], Chunlin Li[†], Yinon Rudich[†], Michal Pardo[†,*]

[†] Department of Earth and Planetary Sciences, Weizmann Institute of Science, Rehovot 76100, Israel

[‡] Department of Chemical Support Services, Weizmann Institute of Science, Rehovot 76100, Israel

[†] These authors have equal contribution

* Corresponding author: michal.levin@weizmann.ac.il

Number of Pages: 10

Number of Figures: 3

Number of Tables: 4

Material and Method

SOA generation in the Potential Aerosol Mass (PAM) oxidation flow reactor (OFR) and OH exposure determination. SOA particles were generated in the OFR by homogeneous nucleation and condensation following OH oxidation of α−pinene and naphthalene[1,2]. Details of the SOA production conditions are listed in Table S1, including initial O_3 concentrations, the relative humidity (RH), and precursor VOCs mixing ratios.VOCs are introduced into the PAM reactor by a gentle N_2 flow through the VOCs bubblers which are temperature controlled. Ozone is generated by irradiating high purity O_2 with a mercury lamp (78−2046−07, BHK Inc., CA, USA) with peak emission at λ= 185 nm outside the PAM reactor. Inside the PAM, $O(^1D)$ radicals are generated by UV photolysis of O_3 using two mercury lamps (82−934−08, BHK Inc., CA, USA) with peak emission at λ= 254 nm. These two lamps are mounted inside Teflon-coated quartz cylindrical sleeves and continually purged with pure nitrogen. Water vapor is introduced into the reactor using a temperature-controlled Nafion membrane humidifier (Perma Pure LIC, NJ, USA). Dry carrier gas of N_2 was mixed with the wet carrier gas (humidified N_2) to provide a controllable relative humidity (RH) in the reactor. A total flow of 4.2 L min^{-1} of N_2 and 0.3 L min^{-1} of O_2 with RH of ~36% was used. The temperature inside the reactor was 22.5±0.3 ℃.

OH radicals are produced via the mechanism as follows:

$$O_3 + h\nu \rightarrow O_2 + O(^1D) (\lambda = 254\ nm) \quad (1)$$

$$O(^1D) + H_2O \rightarrow 2OH \quad (2)$$

In the case of SOA generation with NOx, 90 mL min^{-1} N_2O was added to the PAM reactor. The NO and NO_2 are produced through the following mechanism:

$$O(^1D) + N_2O \rightarrow 2NO \quad (3)$$

$$O_3 + NO \rightarrow O_2 + NO_2 \quad (4)$$

For the fresh SOA produced, SO_2 (50 ppm) was added to the PAM reactor before turning on the UV lamps to sustain an initial SO_2 concentration of ~ 100 ppb. After the UV lamps on, we measured the final SO_2 concentration coming out of the PAM reactor, and then the OH exposure ($\int [OH] dt$) can be calculated as[3]:

$$\int [OH] dt = \frac{1}{k_{OH+SO2}} ln\left(\frac{[SO_2](initial)}{[SO_2](final)}\right) \quad (5)$$

A recent study by Peng *et al.* has developed a model to simulate the atmospheric fate of the RO_2 radicals in the PAM reactors[4,5]. Using their model, we estimate the relative contribution of RO_2 + NO pathway to the RO_2 + HO_2 pathway in the fate of RO_2 radical.

Cell culture, exposure system and optimization of the exposure. Human lung adenocarcinoma epithelial cell line A549 (ATCC catalog no.CCL-185) were exposed in the CULTEX RFS system. Briefly, 24 h prior to the exposure, cells were seeded on Corning Trans-well inserts with microporous membrane (growth area ~12 mm^2, 0.4 μm pore size, Corning Transwell, USA) with an optimized density of 3×10^5 cells mL^{-1}. Before exposure, the cell medium was removed from the apical and basolateral sides. The exposure medium was supplemented with HEPES without FBS. Exposure times varied between 1 to 6 hours. The maximal exposure time and flow parameters were validated by measuring cell viability under clean flow. The gas flow rates through the Trans-wells and the main outlet were

adjusted to 10 ml min^{-1} and 1 L min^{-1}, respectively. As positive control, cells were exposed to copper sulfate particles generated by atomizing copper sulfate solutions (0.03 to 3 gr L^{-1}) using a constant output atomizer (TSI)[6]. As negative control, the cells were exposed to OFR-atmosphere that passed through a HEPA filter.

To determine the possible range of exposure times, A549 cells were exposed to clean air for up to 24 hours. Exposure to clean air for up to six hours did not cause significant changes in cell viability while more significant changes were observed after 8 hours exposure. Efficient particle deposition was achieved with a unipolar electrodeposition device (EDD). The EDD voltage was optimized for SOA particle deposition by measuring the particle size distribution downstream of the CULTEX chambers. Applying the deposition voltage (between -100 and -300 V), decreased cells survival (~40%) compared to the incubator control, without significant changes between the various voltages applied. Thus, the optimal voltage for the SOA exposure experiments was set to -300 Volts.

Results

Table S1. Summary of the Initial Conditions for SOA Experiments.

SOA types	O_3 (ppm)	RH (%)	VOCs (ppb)	N_2O (%)	Aging time (days)	RO_2+NO / RO_2+HO_2
naphthalene SOA	40.0	36%	250	0	2.2[a]	0
				2	3.2[b]	0.21
				0	11[a]	0
α-pinene SOA	36.0	36%	128	0	2.3[a]	0
				2	3.2[b]	0.24
				0	9.8[a]	0

[a] aging time determined by SO_2 decay method

[b] aging time determined by a model based on ozone concentrations and so on.

Table S2. Density and chemical composition (elemental ratios) of fresh, aged and with NOx conditions of naphthalene and α-pinene- derived SOA.

SOA precursor	Naphthalene			α-pinene		
SOA type	Fresh	aged	With NOx	Fresh	aged	With NOx
Aging time (days)	2.2±0.3	11.0±1.1	3.2±0.3	2.3±0.5	9.8±0.5	3.2±0.5
Density (gr cm^{-3})	1.29±0.00	1.35±0.02	1.40±0.02	1.14±0.02	1.23±0.02	1.28±0.01
H:C	1.03±0.01	1.04±0.01	1.08±0.01	1.59±0.01	1.46±0.01	1.57±0.01
O:C	0.72±0.02	1.17±0.02	1.01±0.03	0.51±0.01	0.69±0.04	0.59±0.02

Table S3. Exposed components during the exposure experiments.

SOA precursor	Naphthalene			α-pinene		
SOA type	Fresh	aged	With NOx	Fresh	aged	With NOx
Particle mass (μg cm^{-2})	9.8±1.1	8.0±0.5	8.6±0.9	9.7±3.8	11.0±1.3	3.9±0.1
Total organic peroxides (nmol cm^{-2})	50.5±5.7	109.9±6.6	48.0±4.8	35.9±14.2	81.3±9.5	14.9±0.4
Total superoxide (nmol cm^{-2})	0.3±0.1	0.1±0.0	0.1±0.0	0.9±0.2	1.0±0.4	1.1±0.3

Table S4. SOA characterization: organic peroxide and ROS production.

SOA precursor	Naphthalene			α-pinene		
SOA type	Fresh	aged	With NOx	Fresh	aged	With NOx
Total organic peroxides ($nmol\ \mu g^{-1}$)	5.17±1.81	13.80±2.37	5.56±1.27	3.72±1.87	7.39±1.64	3.87±2.26
Total ROS radicals ($nmol\ \mu g^{-1}$)	0.019 ~ 0.049	0.007 ~ 0.013	0.0134 ~ 0.030	0.079 ~ 0.159	0.082 ~ 0.230	0.299 ~ 0.596
BMPO-OH ($nmol\ \mu g^{-1}$)	0.000 ~ 0.005	0.000 ~ 0.007	0.000 ~ 0.019	0.018 ~ 0.033	0.040 ~ 0.090	0.105 ~ 0.210
BMPO-OOH ($nmol\ \mu g^{-1}$)	0.019 ~ 0.044	0.006 ~ 0.007	0.011 ~ 0.013	0.061 ~ 0.126	0.042 ~ 0.140	0.194 ~ 0.386

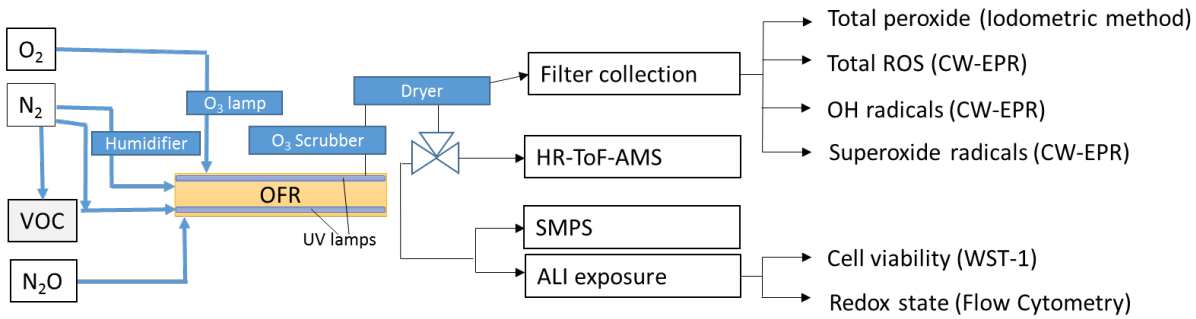

Figure S1. Schematic representation of the experiment: secondary organic aerosol (SOA) production, sampling, cell exposure system, and chemical and biological effects analyses. SOA are produced in an oxidation flow reactor (OFR), which is supplied by ozone, humidified nitrogen (relative humidity 35-38%), precursor volatile organic compounds (VOC) flow, and nitrous oxide (N_2O) as a source of NOx when necessary. After production, the SOA passed through a dryer, collected on a Teflon filter and analyzed for total peroxides content by an Iodometric method, and for ROS by an electron paramagnetic resonance (EPR) instrument for total ROS, OH and superoxide radicals. Simultaneously, the SOA were characterized online by a high-resolution time of flight aerosol mass spectrometer (HR-ToF-AMS), scanning mobility particle sizer (SMPS) and directed to the ALI exposure system (CULTEX RFS system) for the exposure with lung A549 cell. After exposure, the cells were removed and investigated for cytotoxicity and redox state by flow cytometry. Cells' viability was studied by WST-1 test.

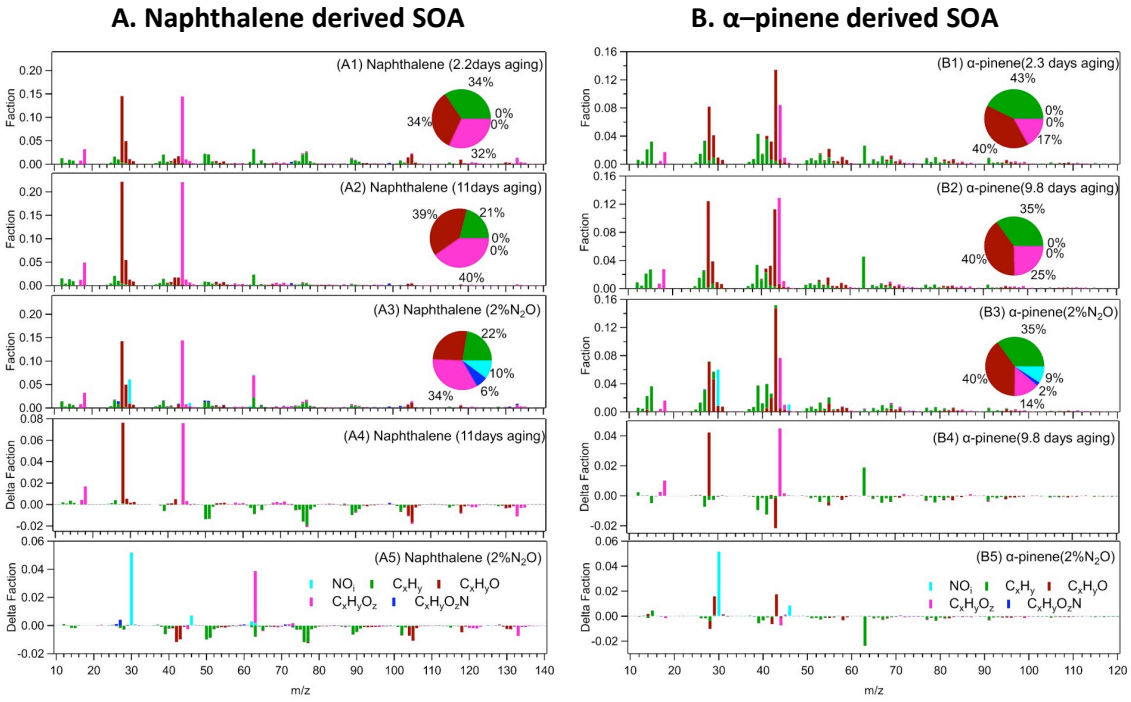

Figure S2: Mass spectra of fresh, aged, and NOx conditions of (A1–A3) naphthalene and (B1–B3) α-pinene derived SOA obtained by HR-TOF-AMS. The difference of the mass spectra compared to that of fresh SOA are also shown for naphthalene and (A4–A5) and α-pinene (B4–B5) derived SOA. The pie charts show the average bulk chemical information including organic-related fragments (grouped as $C_xH_y^+$, $C_xH_yO^+$, $C_xH_yO_z^+$, $C_xH_yO_zN^+$, and NO_i^+, where x, y, i ⩾ 1, z> 1). Large portions of more oxidized species ($C_xH_yO_z^+$) were observed in aged SOA and large fractions of nitrogen-containing species ($C_xH_yO_zN^+$ and NO_i^+) were detected in SOA produce under NOx condition.

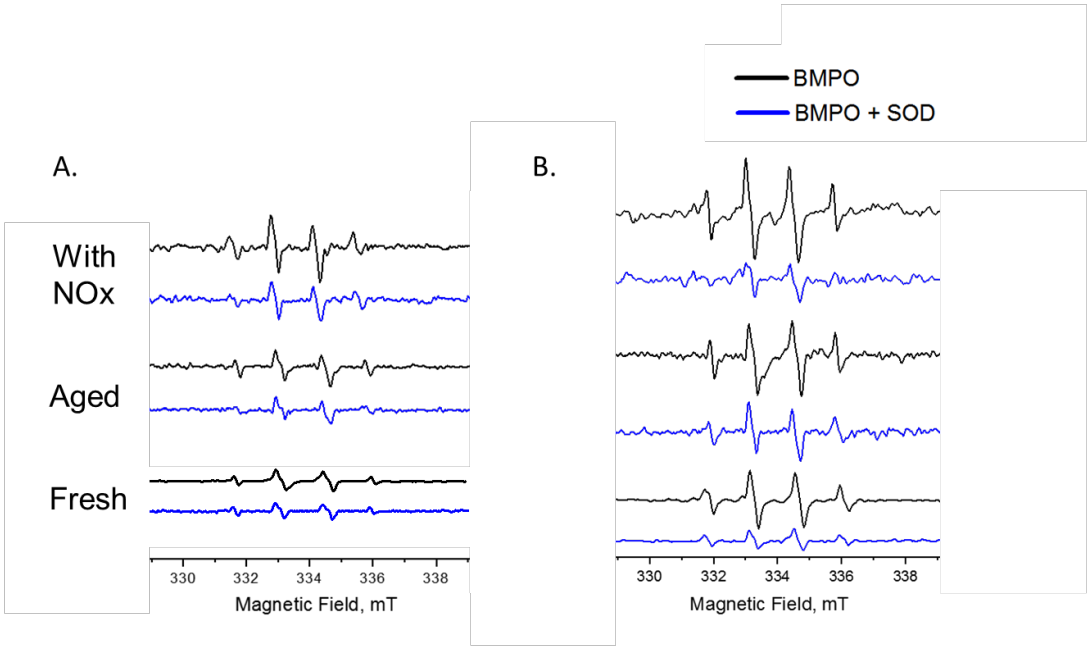

113

114 **Figure S3.** EPR spectra of SOA radicals in (A) naphthalene and (B) α-pinene SOA
115 collected on filters and extracted in water. Reaction with BMPO resulted in the total BMPO
116 bound radicals. Reaction with BMPO and superoxide dismutase (SOD) together resulted
117 in BMPO-OH adduct from hydroxyl radical only (blue spectra).

References

(1) Kang, E.; Root, M.; Toohey, D.; Brune, W., Introducing the concept of potential aerosol mass (PAM). *Atmos. Chem. Phys.* **2007,** *7*, (22), 5727-5744.

(2) Lambe, A. T.; Ahern, A. T.; Williams, L. R.; Slowik, J. G.; Wong, J. P. S.; Abbatt, J. P. D.; Brune, W. H.; Ng, N. L.; Wright, J. P.; Croasdale, D. R.; Worsnop, D. R.; Davidovits, P.; Onasch, T. B., Characterization of aerosol photooxidation flow reactors: heterogeneous oxidation, secondary organic aerosol formation and cloud condensation nuclei activity measurements. *Atmos. Meas. Tech.* **2011,** *4*, (3), 445-461.

(3) Li, R.; Palm, B. B.; Ortega, A. M.; Hlywiak, J.; Hu, W.; Peng, Z.; Day, D. A.; Knote, C.; Brune, W. H.; de Gouw, J. A.; Jimenez, J. L., Modeling the Radical Chemistry in an Oxidation Flow Reactor: Radical Formation and Recycling, Sensitivities, and the OH Exposure Estimation Equation. *J. Phys. Chem. A* **2015,** *119*, (19), 4418-4432.

(4) Peng, Z.; Lee-Taylor, J.; Orlando, J. J.; Tyndall, G. S.; Jimenez, J. L., Organic peroxy radical chemistry in oxidation flow reactors and environmental chambers and their atmospheric relevance. *Atmos. Chem. Phys.* **2019,** *19*, (2), 813-834.

(5) Peng, Z.; Palm, B. B.; Day, D. A.; Talukdar, R. K.; Hu, W.; Lambe, A. T.; Brune, W. H.; Jimenez, J. L., Model Evaluation of New Techniques for Maintaining High-NO Conditions in Oxidation Flow Reactors for the Study of OH-Initiated Atmospheric Chemistry. *Acs Earth Space Chem.* **2018,** *2*, (2), 72-86.

(6) Chowdhury, P. H.; He, Q.; Lasitza Male, T.; Brune, W. H.; Rudich, Y.; Pardo, M., Exposure of Lung Epithelial Cells to Photochemically Aged Secondary Organic Aerosol Shows Increased Toxic Effects. *Environ. Sci. Tech. Let.* **2018,** *5*, (7), 424-430.